JOURNAL OF COMPUTATIONAL PHYSICS 117, 132–145 (1995)

A Deterministic Vortex Sheet Method for Boundary Layer Flow

PETER S. BERNARD

Department of Mechanical Engineering and Institute for Advanced Computer Studies, University of Maryland, College Park, Maryland 20742

Received April 4, 1994; revised August 15, 1994

A deterministic vortex sheet method is derived for application to boundary layer flows. Diffusive vorticity exchange is through adaptation of a scheme proposed by Fishelov (*J. Comput. Phys.* **86**, 211, 1990) to vortex elements with a sheet-like structure. Special measures are taken to maintain the integrity of the vortex sheet representation at inflow and solid boundaries. The flow domain is periodically regridded to ensure that it is well covered by vortex elements. In calculations of a startup channel flow and zero-pressure gradient and stagnation boundary layers, smooth instantaneous realizations of the velocity field are achieved which closely match exact results.

1. INTRODUCTION

Vortex methods [21] are well suited, in principle, to the numerical treatment of complex, high Reynolds number turbulent flows by virtue of their minimal susceptibility to numerical diffusion and lack of a fixed grid. Recent advances in developing fast vortex methods [1, 2, 16, 17] and the parallel implementation of vortex algorithms on supercomputers [24] have effectively eliminated many past limitations on the number of vortex elements that can be reasonably employed in simulations. It has also become increasingly evident [9] that simulations of three-dimensional turbulence may not require resolution beyond that of the principal energy containing vortical structures. Thus, in analogy to large eddy simulations, the computational requirements of a successful turbulent flow model may be eased by removal of "subgrid" vortices [8]. The result is that calculations may now be feasible with sufficient scale resolution to provide a physically accurate simulation of three-dimensional turbulent flow [18].

The physics of the turbulent boundary layer is governed by transport deriving from self-replicating quasi-streamwise vortices [4] coupled to strong wall-normal viscous diffusion of spanwise vorticity. To successfully model such flows, vortex element methods must faithfully represent each of these phenomena. A variety of three-dimensional vortex methods have been proposed [21] which may be capable of modeling the inviscid dynamics of coherent vortical structures. Viscous diffusion of vorticity, on the other hand, has tended to be modeled by imposing a random walk on vortex elements [5–7, 14, 15]. This has a chaotic influence upon the simulated velocity field which can overwhelm the naturally occurring irregular eddying motion found in real turbulent flow [15]. Consequently, it appears to be essential that a deterministic scheme be used for modeling vorticity diffusion in the context of vortex element simulations of turbulent boundary layer flows.

The focus of this work is the development of a deterministic vortex method capable of providing accurate instantaneous simulations of two-dimensional boundary layers. This will also serve, after suitable generalization, as a methodology for modeling wall-normal vorticity diffusion in the context of a three-dimensional vortex method treatment of turbulent boundary layers. The approach is a nonrandom reformulation of Chorin's [7] vortex sheet method in which the elements are given a smooth structure such as is now routinely applied in vortex blob calculations [21]. In particular, fluctuations caused by the velocity discontinuity associated with zero thickness sheets is avoided. Diffusion of vorticity is accommodated through an adaptation to vortex sheets of the deterministic exchange process developed by Fishelov [13].

Several alternative approaches toward a deterministic description of diffusion have been introduced in recent years. These include approximating the Laplacian by an integral operator evaluated on the vortex elements [10–12, 19, 27], directly estimating the Laplacian on the free Lagrangian grid formed by the vortex particles [22], and introducing an effective diffusion velocity [20]. In the Fishelov scheme [13] viscous transfer between vortex elements is arranged by applying the diffusion operator to the smoothed vorticity field. As will be seen below, this method is readily adaptable to the geometry of sheets and the presence of a solid boundary, and it is perhaps the most natural of the deterministic methods to implement within the context of the current scheme.

Deterministic vortex algorithms require that that part of the flow domain containing the support of the vorticity be completely covered by vortex elements at all times. For the present scheme this implies that vortex sheets near the solid boundary must be allowed to change size in order to prevent the formation of regions that are free of vortices. This has another consequence—in common with other Lagrangian methods [14, 22]—that the flow field be periodically regridded or "resheeted" to restore uniformity to the distribution and size of the elements.

0021-9991/95 $6.00

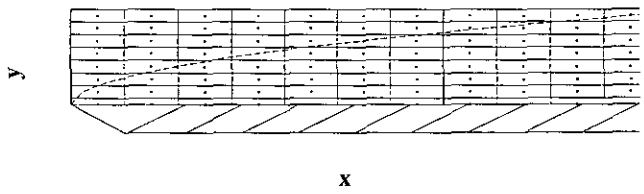

FIG. 1. Initial configuration of sheets for boundary layer calculations.

An examination of some of the implications of this procedure is given below.

An algorithm for boundary layer simulation via smooth vortex sheets is presented in the next section, followed by an analysis of the kinematical computation of velocities from given positions and intensities of the vortex elements. A treatment of boundaries is then given, after which the performance of the scheme is analyzed in the context of several particular flows. These include the transitory development of a channel flow in which the time accuracy of the method is investigated, a zero-pressure gradient Blasius boundary layer and the boundary layer developing downstream of a stagnation point, i.e., the Falkner–Skan similarity solution corresponding to a linearly increasing outer flow velocity [23]. In the last section conclusions are presented.

2. VORTEX SHEET ALGORITHM

The evolution of the vorticity field, $\omega(\mathbf{x}, t)$, in two-dimensional flow is governed by the transport equation

$$\frac{\partial \omega}{\partial t} + \mathbf{u} \cdot \nabla \omega = \frac{1}{R} \nabla^2 \omega, \tag{1}$$

where R is the Reynolds number and $\mathbf{u} = (u, v)$ is the velocity field. In the present scheme, approximate solutions to (1) are obtained in the form of collections of N vortex sheets or "tiles" of large aspect ratio l_i/h_i, where $2l_i$ and $2h_i$ are the width and height of the ith tile, respectively. The vortex sheets are assumed to have uniform vorticity, $\omega_i(t)$, and to convect with the velocity of their centers—generally without change of size and shape. For most of the sheets, h_i and l_i are assigned common constant values h and l, respectively, equal to the initial dimensions of the vortex element field. The typical vortex sheet representation at the start of a boundary layer calculation is illustrated in Fig. 1. For reasons which will subsequently become evident, sheets at the inflow boundary and close to the wall are permitted to increase in size after each convective step. For these special elements, h_i and l_i are time dependent.

Figure 1 shows a layer of sheets of half thickness arranged along the wall. These elements are kept stationary during the calculation, consistent with the view that they are full sized sheets whose centers are on the wall surface and, hence, non-moving. The vorticity of these elements is assigned at each time step in such a way as to satisfy the no-slip boundary condition.

The convection term on the left-hand side of (1) is satisfied by having the positions $\mathbf{x}_i(t) = (x_i(t), y_i(t))$ of the vortex sheets obey the kinematic equation

$$\frac{d\mathbf{x}_i}{dt} = \mathbf{u}(\mathbf{x}_i(t), t). \tag{2}$$

For the results presented below, the explicit first-order scheme

$$x_i^{n+1} = x_i^n + \Delta t u_i^n \tag{3}$$

$$y_i^{n+1} = y_i^n + \Delta t v_i^n \tag{4}$$

is used to advance the positions of the vortex sheets, where x_i^n and y_i^n are discrete approximations to $x_i(n\ \Delta t)$ and $y_i(n\ \Delta t)$, respectively, $u_i^n \approx u(\mathbf{x}_i^n, n\ \Delta t)$, $v_i^n \approx v(\mathbf{x}_i^n, n\ \Delta t)$, and Δt is the time step of the calculation. Some computations were also made using a second-order Runge–Kutta approximation to (2), although these did not lead to any noticeable differences in the computed results. This may be due to the limited scope of the applications considered here; e.g., high order approximations to (2) may be of more significance in complex nonsteady flows.

To take into account vorticity diffusion in the boundary layer, Eq. (1) may be interpreted in a Lagrangian sense as

$$\frac{d\omega_i}{dt} = \frac{1}{R} (\nabla^2 \omega)_i, \tag{5}$$

where $(\nabla^2\omega)_i$ denotes evaluation of $\nabla^2\omega$ at the location of the ith vortex. Following the development in Fishelov [13], ω may be convolved with a cutoff function ϕ_δ to obtain the approximate representation

$$\omega \approx \phi_\delta * \omega \tag{6}$$

from which the estimate

$$\nabla^2 \omega \approx \nabla^2 \phi_\delta * \omega \tag{7}$$

follows. Substituting (7) into (5) and evaluating the convolution integral by summing over the collection of sheets, a basis for a deterministic model of vorticity diffusion is provided. For a first-order explicit approximation to the left-hand side of (5) there follows that

$$\omega_i^{n+1} = \omega_i^n + \frac{\Delta t}{R} \sum_j \omega_j^n \int_{A_j} \nabla^2 \phi_\delta(\mathbf{x}_i - \mathbf{x}')\, d\mathbf{x}', \tag{8}$$

where A_j is the area occupied by the jth vortical element. For the present study, which is limited to planar flow, ϕ_δ is chosen to be the fourth order cutoff function [3, 13]

$$\phi_\delta(x, y) = \frac{1}{2\pi\delta^2}(4e^{-r^2/\delta^2} - e^{-r^2/2\delta^2}) \tag{9}$$

in which $r^2 = x^2 + y^2$ and δ is the cutoff parameter. Other choices are possible, some of which may have as yet unrecognized advantages.

For unbounded flows Fishelov [13] showed that (8) may be made the basis for a consistent approximation to (5). However, in the presence of boundaries, the radially symmetric structure of ϕ_δ means that part of the support of $\nabla^2\phi_\delta(\mathbf{x}_i - \mathbf{x}')$ in (8) is outside the physical flow domain whenever $\mathbf{x}_i$ is near a wall. Unless some special steps are taken to account for this, the amount of vorticity diffusing to points near the boundary will be distorted. While it is conceivable that a one-sided form of ϕ_δ could be introduced with its support entirely within the flow domain, such developments are beyond the scope of the present study. A simpler method, which appears to work satisfactorily for the calculations described below, is to add contributions to (8) from fictitious tiles covering that portion of the support of $\nabla^2\phi_\delta$ extending beyond the solid boundary. These tiles are taken to be reflections through the wall of physical tiles lying near the surface of the flow domain, with vorticity set by extrapolation of the physical vorticity field through the surface. The strength of a tile at $(x_i, -y_i)$ generated by a tile at (x_i, y_i), where $y = 0$ is the boundary, is given by polynomial extrapolation as

$$\omega(x_i, -y_i) = \omega(x_i, 0) - \frac{y_i}{2h}\left(-\frac{3}{2}\omega(x_i, 0) + 2\omega(x_i, 2h) - \frac{1}{2}\omega(x_i, 4h)\right) + \frac{y_i^2}{4h^2}\left(\frac{1}{2}\omega(x_i, 0) - \omega(x_i, 2h) + \frac{1}{2}\omega(x_i, 4h)\right), \tag{10}$$

where the vorticities on the right-hand side are computed by an interpolation scheme described below. Some computations were also done using linear extrapolation in place of (10), although these proved to be less accurate. As a result of these considerations, it is now to be understood that the summation in (8) covers the necessary set of reflected tiles, each of which has a strength determined from (10).

Evaluation of (8) is much simplified by introducing an approximation designed to take into account the sheet-like structure of the vortical elements. Test calculations showed this to be considerably more accurate and stable than applying simple quadrature formulas. First, consider the contribution to the vorticity of the ith sheet from a vortex whose streamwise position $x_j \approx x_i$. The approximation can then be made,

$$\int_{A_j} \nabla^2\phi_\delta(\mathbf{x}_i - \mathbf{x}')\, d\mathbf{x}' = \int_{x_j - l_j}^{x_j + l_j} dx' \int_{y_j - h_j}^{y_j + h_j} dy'\, \nabla^2\phi_\delta(\mathbf{x}_i - \mathbf{x}') \approx 2h_j \int_{-\infty}^{\infty} dx'\, \nabla^2\phi_\delta(x_i - x', y_i - y_j), \tag{11}$$

where the integration in x' has been legitimately extended to all of $\mathfrak{R}$, since, according to (9), the integrand contains an exponential term depending on $-(x_i - x')^2$, and so it rapidly approaches zero for $x' \neq x_i$. Substituting for ϕ_δ using (9) and carrying out the integration yields

$$\int_{A_j} \nabla^2\phi_\delta(\mathbf{x}_i - \mathbf{x}')\, d\mathbf{x}' \approx \frac{h_j}{\sqrt{\pi}\delta^3}\left[e^{-(y_i - y_j)^2/\delta^2}\, 16\left(\frac{(y_i - y_j)^2}{\delta^2} - \frac{1}{2}\right) + \sqrt{2}e^{-(y_i - y_j)^2/2\delta^2}\left(1 - \frac{(y_i - y_j)^2}{\delta^2}\right)\right] \tag{12}$$

which is valid when $x_i \approx x_j$. At the opposite extreme, when $|x_i - x_j| \gg 0$, the exponential terms in $\nabla^2\phi_\delta$ force it to be small for all x' in A_j. In this case, the integral of $\nabla^2\phi_\delta(\mathbf{x}_i - \mathbf{x}')$ over A_j is negligible. For the general case where $x_i \neq x_j$, the artifice may be taken of multiplying (12) by a factor $\gamma_{ij} \equiv m((x_i - l_i, x_i + l_i) \cap (x_j - l_j, x_j + l_j))/(2l_i)$, where $m(S)$ is the rectilinear measure of the set S. Thus $\gamma_{ij} = 1$ when $x_i = x_j$ and $l_i = l_j$, and $\gamma_{ij} = 0$ if $(x_i - l_i, x_i + l_i) \cap (x_j - l_j, x_j + l_j) = \varnothing$. The introduction of γ_{ij} is motivated by the same considerations as put forth in [7] in the context of the velocity field calculation. Collecting together the previous results, the approximate formula is derived,

$$\omega_i^{n+1} = \omega_i^n + \frac{\Delta t}{R}\sum_j \frac{\gamma_{ij}\omega_j^n h_j}{\sqrt{\pi}\delta^3}\left[e^{-(y_i^n - y_j^n)^2/\delta^2}\, 16\left(\frac{(y_i^n - y_j^n)^2}{\delta^2} - \frac{1}{2}\right) + \sqrt{2}e^{-(y_i^n - y_j^n)^2/2\delta^2}\left(1 - \frac{(y_i^n - y_j^n)^2}{\delta^2}\right)\right], \tag{13}$$

where the sum in (13) is over both the sheets located in the physical domain and the special collection of sheets with strengths given by (10). Since only a relatively small subset of the complete collection of vortical elements intersect $(x_i - l_i, x_i + l_i)$, the complexity of (13) does not make the numerical expense of computing ω_i^{n+1} prohibitive.

Advancement of the vortex elements in time is accomplished by applying (3), (4), and (13) concurrently, so the scheme, as it is implemented here, is fully explicit. This places limits on Δt for stability which may perhaps be avoided by alternative formulations. The applications pursued here, however, are well within the capabilities of the explicit scheme so that the development of other time marching procedures was not pursued further at the present time.

For the purposes of implementing (10), as well as applying boundary conditions and resheeting the flow domain, a scheme is required for computing vorticity at arbitrary points in the flow. Satisfactory performance in this regard is obtained from linear interpolation in the form

$$\omega(\mathbf{x}_i) \approx \frac{\sum_j \gamma_{ij}\theta_{ij}\omega_j}{\sum_j \gamma_{ij}\theta_{ij}}, \tag{14}$$

where $\mathbf{x}_i$ is now meant to denote an arbitrary point in the flow and $\theta_{ij} \equiv m((y_i - h_i, y_i + h_i) \cap (y_j - h_j, y_j + h_j))/(2h_i)$. The denominator of (14) is necessary to compensate for overlap of the vortex elements if this should occur. For a boundary layer flow with the wall at $y = 0$, each of $y_i - h_i$ and $y_j - h_j$ appearing in the definition of θ_{ij} must be set to zero if they happen to be negative. The sum in (14) is just over those vortices in the immediate neighborhood of a point, so it is of minimal computational cost. When $\mathbf{x}_i$ corresponds to the position of a vortex, then (14) gives the exact result $\omega(\mathbf{x}_i) = \omega_i$.

3. VELOCITY FIELD

In the vortex sheet method as originally developed by Chorin [7], the boundary layer approximation $\omega \approx -\partial u/\partial y$ in integrated form,

$$u(x, y) = U(x) + \int_y^{\delta_1(x)} \omega(x, y')\, dy', \tag{15}$$

provides a basis for the calculation of u. Here, $U(x) = u(x, \delta_1(x))$ and $\delta_1(x)$ is the boundary layer thickness at x. For this study, (15) is evaluated by applying a rectangle rule to the integral giving

$$u(x_i, y_i) = U(x_i) + 2h \sum_{j=1}^{M} \omega(x_i, y_i + 2h(j - \tfrac{1}{2})) \tag{16}$$

where $y_i + 2hM \geq \delta_1(x_i)$, and the vorticities in (16) are computed using (14). A prescription for calculating the wall-normal velocity v has also been given [7] based on the integrated two-dimensional continuity equation:

$$v(x, y) = -\frac{\partial}{\partial x} \int_0^y u(x, y')\, dy'. \tag{17}$$

It is helpful in evaluating (17) numerically to first rewrite it as

$$v(x, y) = -y \frac{\partial u}{\partial x} - \frac{\partial}{\partial x} \left(\int_0^y y' \omega(x, y')\, dy' \right), \tag{18}$$

using integration by parts and the relation $\omega = -\partial u/\partial y$. Approximating (18) using central differences for the x derivatives and a rectangle rule for the integral gives

$$v(x_i, y_i) = -y_i \left(\frac{u(x_i + l_i, y_i) - u(x_i - l_i, y_i)}{2l} \right) - (\Delta y)^2 \sum_{j=1}^{M'} (j - 0.5) \left(\frac{\omega(x_i + l_i, (j - 0.5)\,\Delta y) - \omega(x_i - l_i, (j - 0.5)\,\Delta y)}{2l} \right) \tag{19}$$

where $M'\,\Delta y = y_i$, and Δy is chosen to be as close to $2h$ as possible under the constraint that M' is an integer.

To the extent that (16) and (19) depend on the boundary layer assumption $\omega = -\partial u/\partial y$, they (or their three-dimensional analogues) cannot be expected to accommodate the full range of motions in the near wall region of turbulent flow. Consequently, it is necessary to also consider more generally applicable relations for the kinematic determination of velocities. In particular, now considering three-dimensional flow, the Biot–Savart integral

$$\mathbf{u}(\mathbf{x}, t) = \int_{\mathbb{R}^3} K(\mathbf{x} - \mathbf{x}') \boldsymbol{\Omega}(\mathbf{x}', t)\, d\mathbf{x}', \tag{20}$$

where

$$K(x, y, z) = -\frac{1}{4\pi |\mathbf{x}|^3} \begin{pmatrix} 0 & -z & y \\ z & 0 & -x \\ -y & x & 0 \end{pmatrix} \tag{21}$$

and $\boldsymbol{\Omega}$ is the vorticity vector, may be adapted to computing the velocities associated with sheet-like vortex elements. Following common practice, the singularity in (20) may be removed by replacing K by $K_\eta = \psi_\eta * K$, where ψ_η is a smoothing function equivalent to ϕ_δ introduced previously. As in [14], it will be assumed that

$$\psi_\eta = \begin{cases} 1 & |\mathbf{x}| \geq \eta \\ \dfrac{5}{2}\left(\dfrac{|\mathbf{x}|}{\eta}\right)^3 - \dfrac{3}{2}\left(\dfrac{|\mathbf{x}|}{\eta}\right)^5 & |\mathbf{x}| < \eta, \end{cases}$$

so that

$$K_\eta = \begin{cases} K & |\mathbf{x}| \geq \eta \\ K\left(\dfrac{5}{2} - \dfrac{3}{2}\left(\dfrac{|\mathbf{x}|}{\eta}\right)^2\right) \dfrac{|\mathbf{x}|^3}{\eta^3} & |\mathbf{x}| < \eta, \end{cases}$$

where the cutoff parameter, η, is not necessarily the same as δ, appearing in (9). With this modification (20) may be written as

$$\mathbf{u}(\mathbf{x}, t) = \sum_j \int_{V_j} K_\eta(\mathbf{x} - \mathbf{x}') \boldsymbol{\Omega}_j(\mathbf{x}', t)\, d\mathbf{x}', \tag{22}$$

where V_j is the volume occupied by the jth element. Where appropriate, the summation in (22) is assumed to include image vortex sheets used in enforcing the nonpenetration boundary condition.

For two-dimensional flows, $\boldsymbol{\Omega} = (0, 0, \omega)$, and the vortex elements in (22) may be considered to extend indefinitely in the spanwise direction. Under this circumstance, the z integra-

tion over $\Re$ can be carried out explicitly. A closed form solution can also be obtained for the streamwise integration over the limits $x_j - l_j$, $x_j + l_j$ of the vortex sheet in V_j. Finally, the y integral can be modeled by evaluating the integrand at $y' = y_j$. The final result is the nonlocal relations

$$u(\mathbf{x}_i, t) = \sum_j U_{ij}\omega_j \tag{23}$$

$$v(\mathbf{x}_i, t) = \sum_j V_{ij}\omega_j, \tag{24}$$

where U_{ij}, V_{ij} are the respective contributions of the jth vortex sheet to the u and v velocity components at $\mathbf{x}_i$. These are given formally by

$$\begin{aligned} U_{ij} = -\frac{h_j}{\pi}\Bigg[& \tan^{-1}\frac{X_2}{Y} - \tan^{-1}\frac{X_1}{Y} \\ & - \left(\tan^{-1}\frac{X_2}{YR_2} - \tan^{-1}\frac{X_1}{YR_1}\right) \\ & + \frac{Y}{2}\Bigg\{\frac{3}{4}\left(\frac{7}{3} - Y^2\right)(X_2R_2 - X_1R_1) \\ & + \frac{1}{2}(X_2R_2^3 - X_1R_1^3) \\ & + \frac{3}{4}\left(Y^4 - \frac{10}{3}Y^2 + 5\right)\left(\tan^{-1}\frac{X_2}{R_2} - \tan^{-1}\frac{X_1}{R_1}\right)\Bigg\}\Bigg] \end{aligned} \tag{25}$$

$$\begin{aligned} V_{ij} = \frac{h_j}{\pi}\Bigg[& \ln\frac{r_2}{r_1} + (R_1 - R_2) + \frac{1}{3}(R_1^3 - R_2^3) \\ & + \frac{1}{5}(R_1^5 - R_2^5) + \ln\frac{1 + R_2}{1 + R_1} - \frac{1}{2}\ln\frac{1 - R_2^2}{1 - R_1^2}\Bigg], \end{aligned} \tag{26}$$

where

$$R^m = \begin{cases} \sqrt{1 - r_m^2}, & r_m < 1 \\ 0, & r_m \geq 1 \end{cases}, \qquad m = 1, 2$$

$$r_m^2 = X_m^2 + Y^2, \qquad m = 1, 2,$$

$$X_1 = (x_i - x_j - l_j)/\eta$$

$$X_2 = (x_i - x_j + l_j)/\eta$$

and

$$Y = (y_i - y_j)/\eta.$$

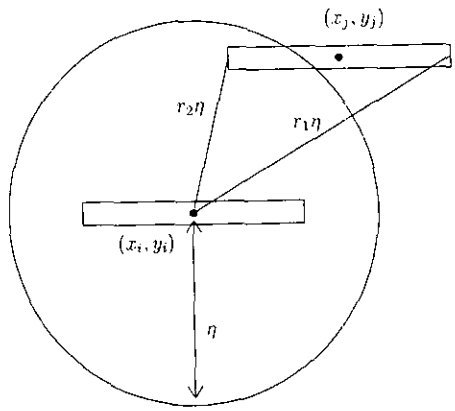

FIG. 2. Geometry of sheet interactions.

A geometrical interpretation of r_1 and r_2 is given in Fig. 2. Despite the apparent complexity of these formulas, for the great majority of vortex interactions, r_1, $r_2 \geq 1$, in which case (25) and (26) simplify to

$$U_{ij} = -\frac{h_j}{\pi}\left(\tan^{-1}\frac{X_2}{Y} - \tan^{-1}\frac{X_1}{Y}\right) \tag{27}$$

and

$$V_{ij} = \frac{h_j}{\pi}\ln\frac{r_2}{r_1}, \tag{28}$$

respectively. Furthermore, to enable calculation with large numbers of sheets, it is likely that a fast multipole summation of (23) and (24) can be developed from (27) and (28).

As was previously encountered in regards to (7), the evaluation of (22) within η of a solid boundary must be done in such a way as to prevent the loss of contributions to $\mathbf{u}$ from that part of the support of ψ_η cut off by the wall. One approach toward this end—which is also fully compatible with the velocity boundary conditions—is to reduce η for sheets near the wall so that the support of ψ_η does not intersect the boundary. Specifically, for flow above a fixed wall at $y = 0$, the contribution of a vortex sheet at y_j to the velocity at y where $0 \leq y \leq y_j$, may be based on insisting that η for the jth sheet be no larger than $|y_j|$. For the velocity at a point $\mathbf{x}_i = (x_i, 0)$ on the wall, this means that the sheet lying immediately over it is forced to contribute to u at the surface via (27) and not (25). In this case, the difference in arctangent terms in (27) is essentially π, so that the contribution to the streamwise wall velocity is $-h_i\omega_i$, i.e., exactly what is expected from a physical analysis of the vortex sheet.

The consistency of (16) and (23) in computing u and (19) and (24) in computing v may be tested by comparing their predictions against exact similarity results for a zero pressure gradient boundary layer. In this, the initial sheet arrangement

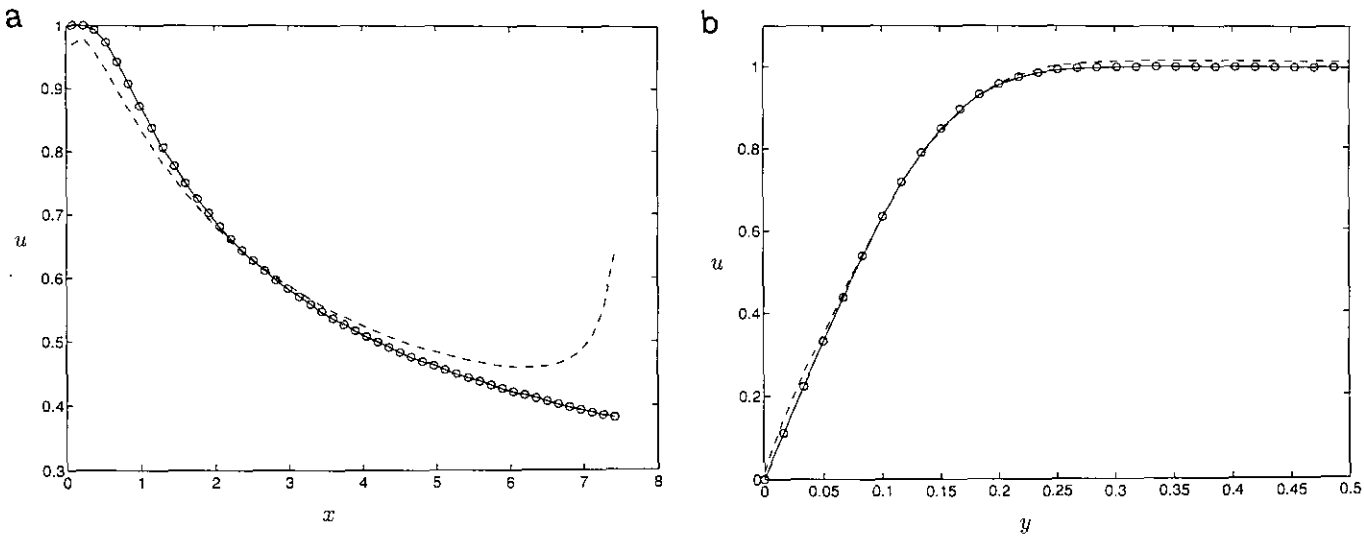

FIG. 3. Tests of u predictions: ———, Eq. (16); – – –, Eq. (23); and ○, Blasius solution. (a) $y = 0.1$; (b) $x = 2.5$.

in Fig. 1 is used wherein each vortex element is assigned its "exact" vorticity. The latter is obtained from cubic spline interpolation of the tabulated values given by Schlichting [11]. For this and subsequent discussions of boundary layer flow, lengths are assumed scaled by a streamwise length, L, and velocities by the free stream velocity, U_∞. The Reynolds number $R = U_\infty L/\nu$, and calculations are performed in the nondimensional flow domain $0 \le x \le x^*$, $0 \le y \le y^*$, where $x^* = 7.5$ and $y^* = 6.4\sqrt{x^*/R}$. y^* is chosen to be large enough to contain the complete lateral boundary layer growth through position x^*. For the present purposes, $R = 1000$, $N = 1200$ (i.e., a 60×20 arrangement), $l = 0.05$, and $h = 0.0138$. Here and in the following, $\eta = C_\eta\sqrt{h}$ with $C_\eta = 0.5$. Figures 3a and b show the u predictions on the lines $y = 0.1$ and $x = 2.5$, respectively, while Figs. 4a and b contain similar plots of the v velocity.

It is clear from Fig. 3a that (16) captures the streamwise velocity with high accuracy along the entire length of the boundary layer, including both the leading edge and the exit plane. In contrast, (23) is reasonably accurate only until $x \approx 4$, after which it diverges from the Blasius solution, finally becoming entirely unphysical at $x \approx 7$, where it sharply rises. The poor performance of (23) reflects the absence of contributions from vorticity lying beyond x^*, a flaw which cannot be simply corrected in a boundary layer calculation, since the needed vorticity can only be obtained with knowledge of the velocity in the

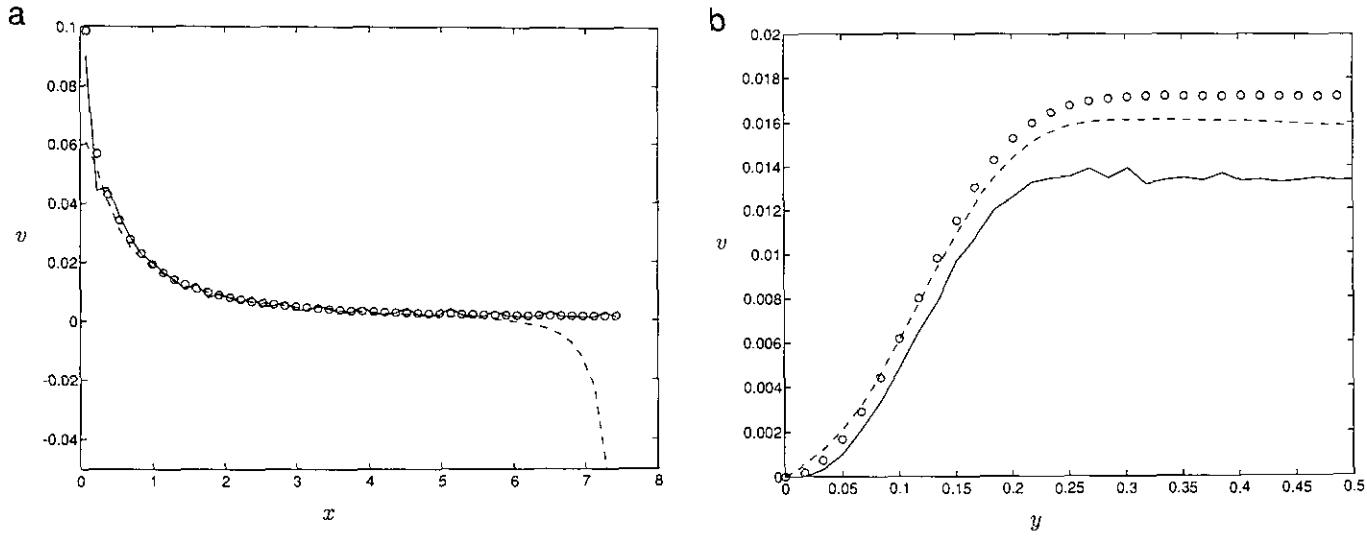

FIG. 4. Tests of v predictions: ———, Eq. (19); – – –, Eq. (24); and ○, Blasius solution. (a) $y = 0.1$; (b) $x = 2.5$.

same region, which itself requires the vorticity further downstream and so on. Figure 3a also shows that (23) is somewhat inaccurate at the leading edge of the boundary layer. This may be attributed to the failure of the Blasius solution to accurately account for the vorticity field at and around the upstream end of the flat plate. For example, the Blasius similarity solution predicts that v and ω are singular at $x = 0$.

The accuracy of (16) also holds up in the cross stream direction as shown in Fig. 3b, while (23) shows small deviations from the exact velocity near the wall and outer edge of the boundary layer. In the former case, these may be partly a result of the wall treatment of ψ_η, while the latter may be a result of excluding long-range contributions from vorticity outside the computational box.

In the case of the wall-normal velocity, Figs. 4a and 4b show that each of the formulas (19) and (24) are potentially useful, but neither is free of problems. As in the case of (23), (24) suffers from the finite extent of the calculation domain by diverging from the correct solution, although in this instance, it remains accurate to at least $x \approx 6$. Near the leading edge it deviates from the unphysical singularity of the Blasius solution. According to Fig. 4b, (24) is fairly accurate across the boundary layer, although it underpredicts v near the outer edge and slightly overpredicts it at the wall. These errors are likely due to the long-range effect of the missing downstream vorticity, the form of ψ_η and the tile resolution in the wall-normal direction. Note that the nonpenetration boundary condition has been identically satisfied with the use of image vortex sheets.

Equation (19) also displays some undesirable properties in its representation of v, although the overall trend is captured. Particularly evident in Figs. 4a and b is its susceptibility to oscillations. The effect of these in calculations is minimal, however, since their relative amplitude in comparison to the streamwise velocity is small. It should be remarked that for sufficiently coarse streamwise resolution v associated with (24) is also subject to significant oscillations; thus there is a minimum density of elements in the streamwise direction necessary for (24) to yield the smooth prediction displayed in Fig. 4b.

It is clear that between the two approaches, only (16) and (19) are useful near the exit region of boundary layer flows. Equations (23) and (24) may be used only if steps are taken to counter their erroneous predictions near the downstream edge, e.g., by replacing them by (16) and (19) in the outflow region. Calculations of boundary layers described below use (16) exclusively for u, while v is computed with the hybrid approach for the Blasius flow and via (19) for the Falkner–Skan flow. Equation (23) is readily used in computations of periodic channel flow since edge effects are easily eliminated through the use of periodic streamwise extensions of the flow domain. In summary, it appears that there are circumstances when each of the velocity formulas may be useful. However, for treatment of turbulent flow it is likely that only three-dimensional extensions of (23) and (24) would be appropriate, since they will not depend on the boundary layer assumption.

4. BOUNDARY CONDITIONS

The no-slip condition is satisfied locally by assigning vorticity to the row of half thickness sheets kept fixed along the solid wall. If (16) is employed in computing u, then after the computation of $\mathbf{x}^{n+1}$ and ω^{n+1} from (3), (4), and (13), the wall vorticity at the ith sheet is updated via the first-order formula

$$\omega(x_i, 0) = -\frac{u(x_i, h)}{h}, \tag{29}$$

where $u(x_i, h)$ is computed from (16). If u is determined from (23), then satisfaction of the no-slip condition requires setting (23) equal to zero at the location of each of the wall sheets. This yields a coupled system of equations which may be solved for the wall vorticities.

Unlike the random vortex method, deterministic approaches require vortex elements—even possibly of zero vorticity—to be present at all points of the flow that may be the recipient of vorticity from viscous transfer. As a result, special care must be taken, particularly at boundaries, to ensure that no artificial voids in the element population arise which would distort the diffusion process. For boundary layer flow this chiefly means making special provision for the upstream influx of vorticity-free fluid and allowing for the drift of fluid away from the solid boundary. In each of these cases, the integrity of the vortex sheet calculation can be maintained by permitting special groups of vortex elements to deform according to the local flow conditions.

At an inflow boundary, such as $x = 0$ in Fig. 1, the movement of new fluid into the computational domain can be accounted for by allowing the column of sheets with ends at $x = 0$ to elongate from one time step to the next. This may be conceptualized as a two-step process in which the sheets first convect with the flow, and then the vorticity-free fluid entering the flow domain behind them is appended to their upstream ends. This procedure assures that the tiles always possess large aspect ratios so that the validity of the approximations in (13), (23), and (24) remain valid. When one of these sheets reaches a length $>4l$, a sheet of length $2l$ is subtracted from it at its downstream end—which is then treated like the other elements—while the remaining part of the original sheet becomes a new boundary element with the capacity to lengthen and eventually divide again in the future. Since the growth of the boundary sheets is due to the infusion of zero vorticity fluid, it is necessary to reduce their vorticity accordingly at each time step. This is formally accomplished by multiplying the updated vorticity ω_i^{n+1} by the factor x_i^n/x_i^{n+1} which effectively averages ω_i between the zero vorticity fluid entering the flow domain and that previously existing in the vortex element.

It is in the nature of the Blasius boundary layer flow for fluid particles to slow and convect away from the surface as they pass over it. This tendency, if left unchecked, creates holes in the vortex element representation near a solid boundary. To

counteract this, each of the elements in the second horizontal row of Fig. 1, i.e., adjacent to the wall elements, are allowed to increase in thickness by a process similar to that for the vortices on the upstream boundary. In this, a sheet is first convected with the flow to position (x_i^{n+1}, y_i^{n+1}), after which the fluid in the gap region between it and the closest wall vortices is appended to it, thereby increasing its thickness. As before, the vorticity of the element is then adjusted to reflect the addition of new fluid. In this instance, after ω_i^{n+1} is computed from (13), it is replaced by the formula

$$\frac{\omega_i^{n+1}2h_i^n + \omega(x_i^n, h)(y_i^{n+1} - h_i - h)}{2h_i^n + (y_i^{n+1} - h_i - h)} \tag{30}$$

representing a weighted average of ω_i^{n+1} and $\omega(x_i^n, h)$—where the latter quantity is the vorticity along the lower boundary of the element before its convection. Note that $y_i^{n+1} - h_i - h$ is the gap width and the denominator in (30) is the new thickness of the vortex sheet.

The vortices in the second row cannot be allowed to grow indefinitely, since they would then eventually have a small aspect ratio. At the same time, it is not feasible to periodically halve them, such as is done along the leading edge, since they do not grow in length along the principal flow direction; i.e., it is likely that newly divided vortices would soon overlap downstream vortices. Consequently, if a regular arrangement of sheet-like vortices is to continually fill all of the flow domain, regridding is inevitable at periodic intervals. Resheeting is done by recreating the arrangement of tiles in Fig. 1 with vorticities determined from (14).

At the downstream boundary, all tiles for which $x_i - l_i > x^*$ are eliminated from the calculation so that the total number of sheets stays approximately constant in time. Since the computation of u, v, ω, and $\nabla^2\omega$ at locations $x > x^* - l$ via (13), (14), (16), (19), and (24) depends on having elements for which $x_i - l_i > x^*$, special measures must be taken to prevent errors in computing flow properties at these positions. In the following computations, this problem is avoided by using linear extrapolation at points $x > x^* - l$. For example, u is computed from

$$u(x, y) = u(x^* - l, y) + \left(\frac{u(x^* - l, y) - u(x^* - 3l, y)}{2l}\right)(x - x^* - l) \tag{31}$$

and similarly for v, ω, and $\nabla^2\omega$. Use of (31) or an equivalent appears to be necessary; e.g., an alternative boundary condition in which streamwise gradients are set to zero for $x > x^* - l$ yields improper boundary layer growth well upstream of x^*.

5. COMPUTED RESULTS

One computational cycle of the deterministic vortex sheet algorithm as it applies to boundary layer flows consists of the following steps. In this it is assumed that x_i^n, y_i^n, and ω_i^n, are known for N vortex sheets covering the flow domain at time $n\Delta t$:

1. Append images of wall proximate sheets—with vorticity determined from (10)—to the N vortices so as to ensure that the support of ϕ_δ is always covered.
2. For interior sheets calculate x_i^{n+1}, y_i^{n+1}, and ω_i^{n+1}, $i = 1, \ldots, N$, using (3), (4), and (13), respectively.
3. Account for new fluid entering the flow domain by modifying the length and vorticity of sheets along inflow boundaries. Divide sheets in two which become greater than $4l$ in length.
4. Accommodate the drift of fluid away from the wall by modifying the width of vortices adjacent to the wall vortices. Recompute the vorticity of these sheets using (30).
5. Update the wall vorticity.
6. Delete vortices which have convected out of the computational domain.
7. Resheet if necessary.
8. Return to step 1.

In problems with periodic streamwise boundary conditions, steps 3 and 6 are unnecessary, since vortices passing through the outflow boundary reappear at the inflow boundary.

Before considering the calculation of boundary layers, a useful test of the algorithm in a simpler setting is its application to the nonsteady channel flow developing from a state of rest after the sudden imposition of a uniform pressure gradient. Denoting the streamwise and wall-normal directions by x and y, respectively, the flow is assumed to be independent of x at all times, i.e., $u = u(y, t)$ and $v = 0$. For a nondimensionalization based on the channel width, d, and the asymptotic average mass flow velocity, U_m, the exact steady state solution in this case is $\omega(y) = -6(1 - 2y)$. Integration of the momentum equation across the channel gives the exact relation

$$\frac{du_m}{dt} = \frac{2}{R}(6 + \omega(0, t)), \tag{32}$$

where $u_m(t)$ is the instantaneous average mass flow velocity and $R = U_m d/\nu$ is the Reynolds number. Note that $u_m(0) = 0$ and $u_m(t) \to U_m$ as $t \to \infty$. A first-order time discretization of (32) may be used to get $u_m(t + \Delta t)$ at the start of each time step calculation. This, in turn, may be used to get the centerline velocity needed in the implementation of (16), or, in the case of (23), a supplementary constant streamwise flow which forces the computed average mass flow velocity to be exactly $u_m(t + \Delta t)$. The condition $v = 0$ is met by (19) and (24) and need not be computed.

If (16) is employed, then the length of the vortex sheets is immaterial and the computation may proceed assuming they are infinitely long. On the other hand, for the application of (23) it is convenient to introduce periodicity in the streamwise direction. Calculations in this study are done assuming a period-

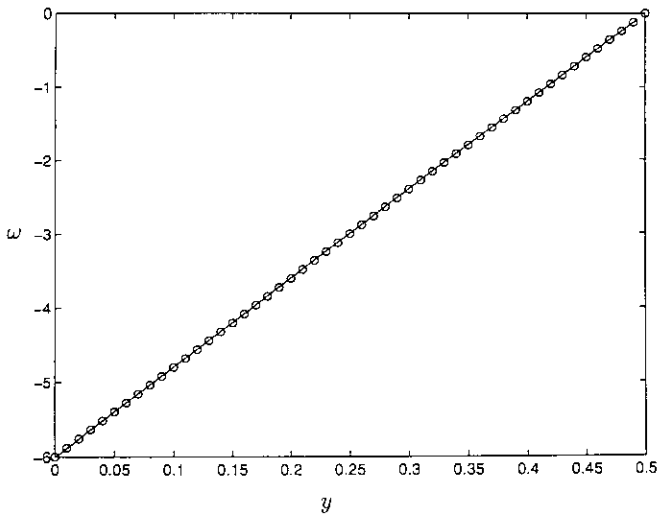

FIG. 5. Steady state vorticity field in channel flow: ———, computed; ○, exact solution.

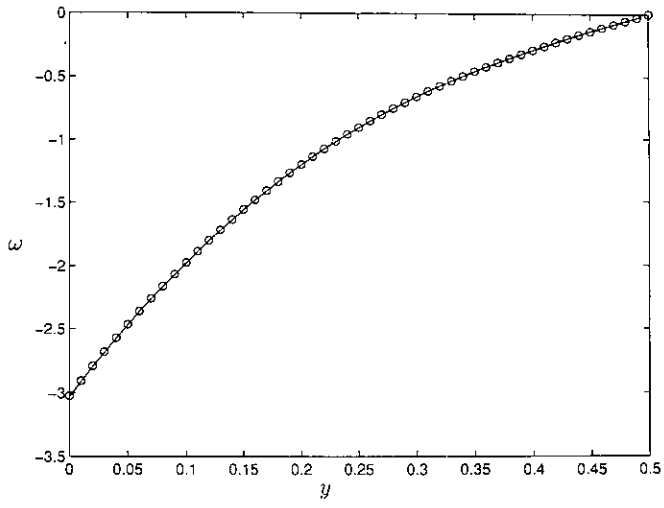

FIG. 7. Vorticity field in channel flow at $t = 50$: ———, computed; ○, exact solution.

icity of $5d$. Several periods, generally three or more, both up and downstream of the computational region are used in the evaluation of (23) to ensure that u is x independent. In particular, this eliminates the edge effect, such as was discussed earlier in reference to Fig. 3. Reflected vortex sheets covering one channel width above and below the channel are introduced to enforce the nonpenetration boundary condition. Inclusion of additional images in this direction has a negligible effect on the results. The streamwise period of the channel is divided into three sheets, while 60 span the width. Adding additional sheets in either direction has no effect upon the computed solution.

Calculations were performed with $R = 1000$ and $\delta = C_\delta\sqrt{h}$, where $C_\delta = 0.2$. The numerical results are identical whether (16) or (23) is used. Figure 5 shows that the asymptotic vorticity field is predicted with very high accuracy. Of perhaps more significance is the degree to which the transient state of the flow is well represented. An indication of this is shown in Fig. 6, comparing the exact time history of u at the point $y = 0.1$ in the channel with that from the present algorithm. The agreement is quite good. Furthermore, Fig. 7 illustrates, through a comparison of the exact and predicted vorticities across the lower half-channel at the intermediate time $t = 50$, that time accuracy is maintained at all points in the flow during the computation. Similar calculations to these were also made assuming impulsive motion of the fluid in the channel, that is, having $u = 1$ as the initial condition. In this case, the initial vorticity discontinuity led to some small discrepancies from the exact transient solution, although the final equilibrium state was unchanged.

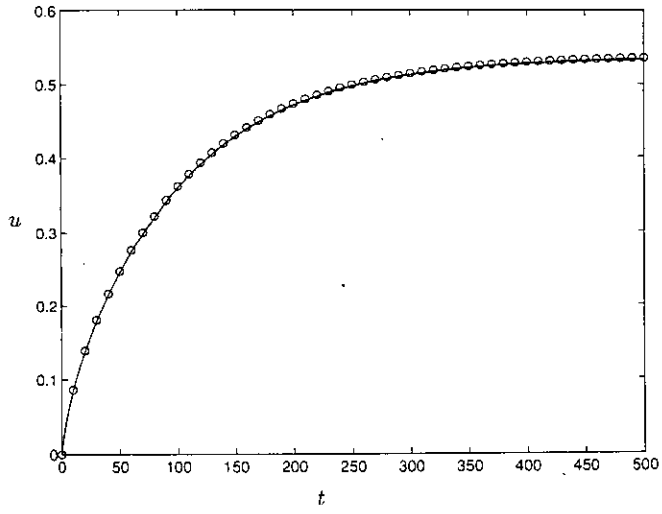

FIG. 6. Time history of u at $y = 0.1$ in channel flow: ———, computed; ○, exact solution.

The Blasius and Falkner–Skan boundary layers were computed by time marching to a steady state after first impulsively moving the fluid in an initially zero vorticity field. The Blasius boundary layer was calculated at $R = 10{,}000$ using a variety of grid sizes and values of the parameters δ and η. The performance of the algorithm in this flow is summarized in Figs. 8–10 comparing the exact similarity solution to numerical calculations using 1200 elements in a 60×20 initial arrangement so that $l/h = 14.3$ and 2700 elements in a 90×30 grid with the same aspect ratio. As the figures show—apart from the singular region near the leading edge—there are only slight differences between these solutions, suggesting that the flow is well resolved in the calculations. As before, $\delta = 0.5\sqrt{\Delta y}$, $\eta = 0.2\sqrt{\Delta y}$, values which ensure that the supports of ϕ_δ and ψ_η overlap several or more sheets in the y direction. The results in the accompanying figures change inconsequentially over a significant range of these parameters.

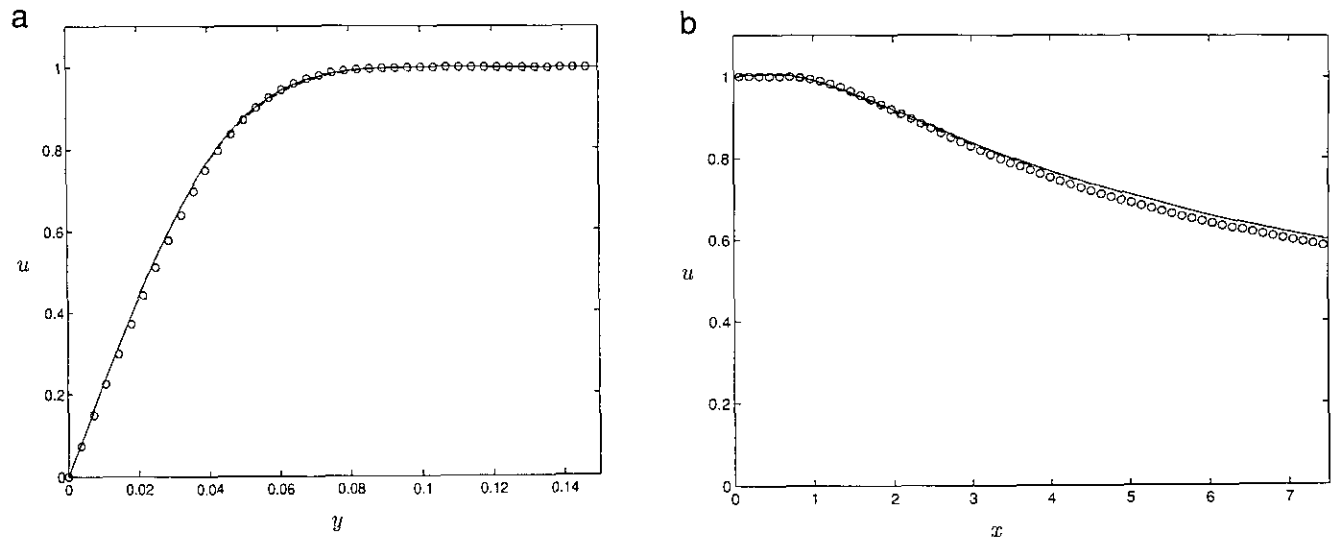

FIG. 8. Comparisons of u predictions in Blasius boundary layer: ---, $N = 1200$; ———, $N = 2700$; and O, Blasius solution. (a) $x = 2.5$; (b) $y = 0.05$.

The streamwise velocity on a wall-normal cut through the boundary layer at $x = 2.5$ is shown in Fig. 8a. The solutions agree well with the Blasius profile. The situation is similar in Fig. 8b, showing u along a streamwise cut on the line $y = 0.05$. Equivalent plots of the wall-normal velocities are shown in Figs. 9a and b. Clearly, the predictions of v are credible, although the relative errors are somewhat greater than in the case of u. However, due to the magnitude of v, the error in absolute terms is actually much lower in this case. Figure 9b shows that near the leading edge, where the variation in v is most significant, enhancing the density of sheets has a beneficial effect on the computations. As in the case of Fig. 4a, Fig. 9b shows that the numerical solution does not mimic the singularity in the Blasius solution. It may be noted that oscillations appear in the v calculation for $x \geq 5$. These may be attributed to the use of (19) in this region as part of the hybrid scheme discussed previously.

Predictions of the vorticity are shown in Fig. 10. On the line $x = 2.5$ in Fig. 10a, ω is closely predicted except at the wall, where it tends to be slightly too large in magnitude. Figure 10b, containing a plot of the vorticity on the wall surface, shows the large variation in ω near the leading edge of the flat plate at this Reynolds number. With refined resolution, the prediction of wall vorticity is substantially improved, suggesting that the singular behavior of the leading edge flow is partly responsible for the disparities in vorticity prediction. It will be seen below

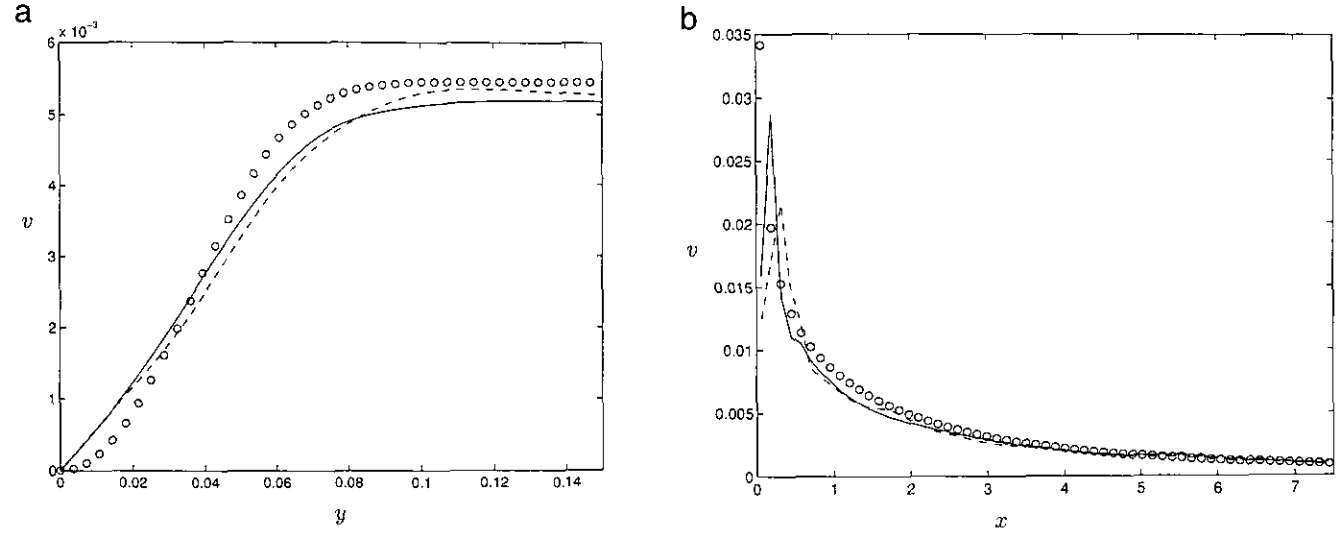

FIG. 9. Comparisons of v predictions in Blasius boundary layer: ---, $N = 1200$; ———, $N = 2700$; and O, Blasius solution. (a) $x = 2.5$; (b) $y = 0.05$.

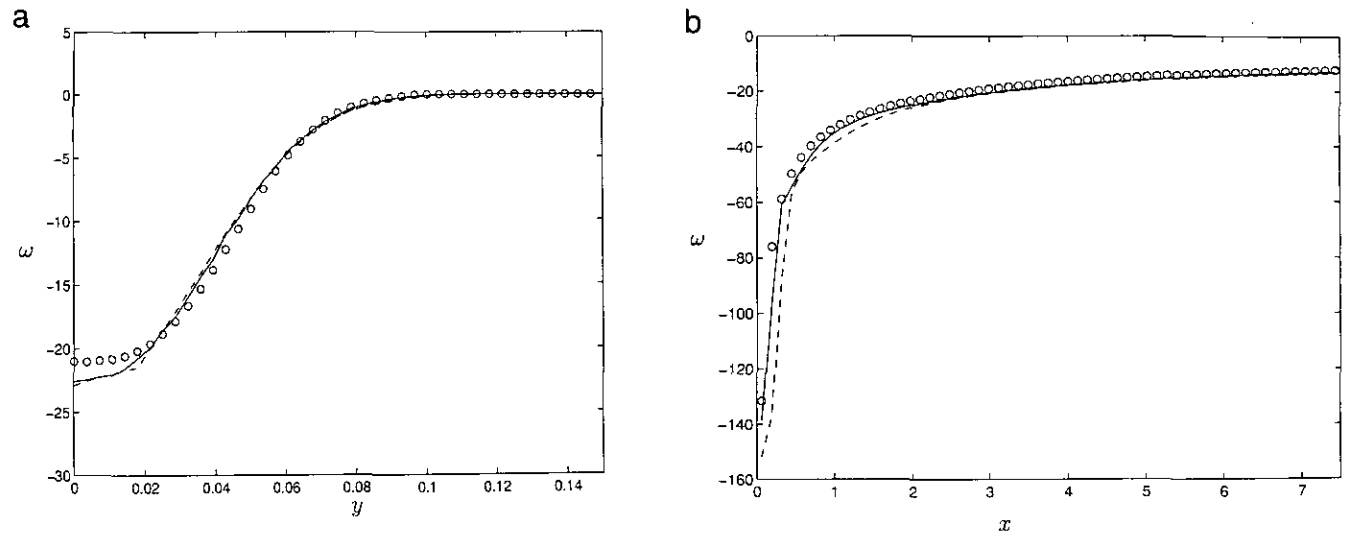

FIG. 10. Comparisons of ω predictions in Blasius boundary layer: ---, $N = 1200$; ———, $N = 2700$; and O, Blasius solution. (a) $x = 2.5$; (b) $y = 0$.

that this view is supported by the stagnation boundary layer calculation where the leading edge flow is smooth and the downstream predictions are very accurate.

The capabilities of the present scheme in describing the boundary layer forming downstream of a stagnation point are illustrated in Figs. 11–13 covering u, v, and ω, respectively. In this case, results are presented for a calculation with $R = 1000$ and $N = 2250$ elements in a 75×30 arrangement. Excellent agreement with the similarity solution for u is found along x and y cuts as shown in Fig. 11. In particular, u is free of the unphysical near-wall behavior which is evident in calculations of this flow using the random sheet method [26]. Similarly, excellent predictions are found in regards to v as displayed in Fig. 12. Figure 13 shows generally very good estimates of the vorticity field, although there is a slight systematic loss of accuracy in the wall vorticity prediction with downstream distance. Since the boundary layer thickness is independent of x for this flow, and the wall vorticity increases linearly with downstream distance, as seen in Fig. 13b, it is clear that the spanwise resolution of the sheet calculation is systematically deteriorating in the streamwise direction. This may account for the loss of accuracy. Greater resolution of sheets may help in counteracting this trend.

Some attention was paid to exploring how the length of the time interval between resheetings, say t_{rs}, affects the computed solutions. It was found that as long as t_{rs} is not too large, the

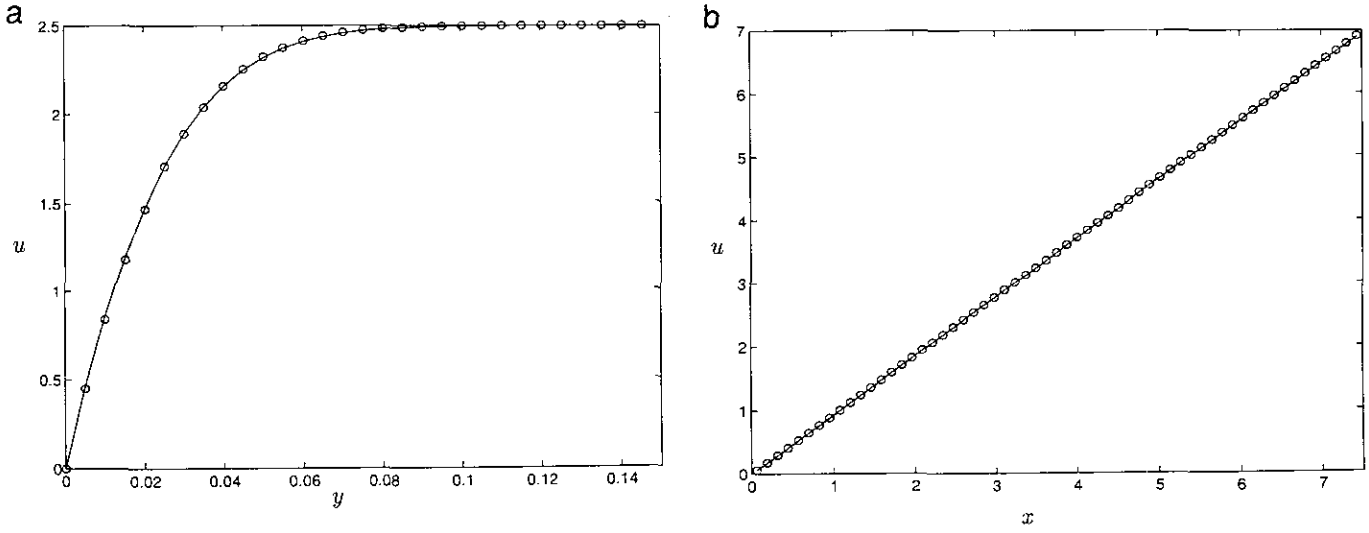

FIG. 11. Comparisons of u predictions in stagnation flow boundary layer: ———, computed; and O, Falkner–Skan solution. (a) $x = 2.5$; (b) $y = 0.1$.

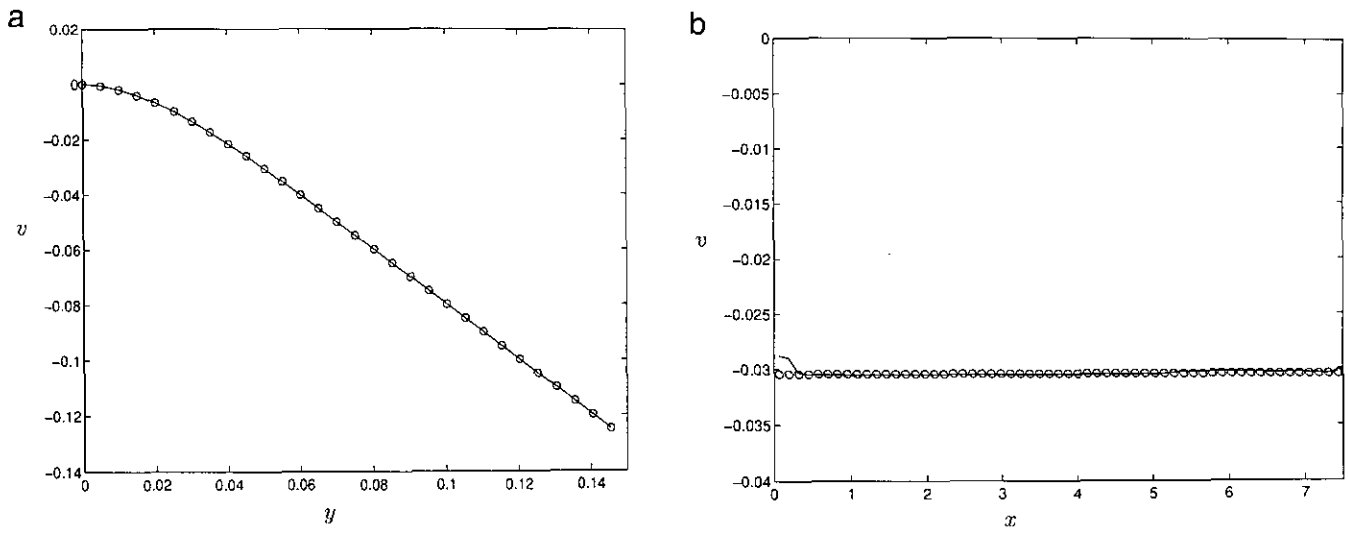

12. Comparisons of v predictions in stagnation flow boundary layer: ———, computed; and O, Falkner–Skan solution. (a) $x = 2.5$; (b) $y = 0.1$.

converged solutions are generally independent of the resheeting process. A useful means of investigating the influence of t_{rs} is through observing time traces of the computed vorticity field at a fixed point for different values of t_{rs}. The results of such a comparison are shown in Fig. 14 for the point $x = 2.5$, $y = 0.025$ in the Blasius boundary layer stimulation at $R = 10{,}000$ with $N = 1200$. The cases $t_{rs} = 0.025$, 0.25, 0.5, 0.75, and 1.0 are considered, where $\Delta t = 0.025$ and $t_{rs} = 0.25$ were used in the previously discussed Blasius boundary layer calculations.

At the largest value, $t_{rs} = 1$, ω has substantial oscillations. Beyond $t = 5$ in Fig. 14 these have a primary period of one which is clearly tied to the resheeting process. Higher frequency disturbances are also visible which originate from other aspects of the numerical algorithm. For example, as many as eight vortex subdivisions would have occurred from vortices on the front boundary during a unit time interval. While the calculation with $t_{rs} = 1$ appears to be stable, its accuracy is unacceptable. For larger values of t_{rs} the solution will ultimately become unstable, with the appearance of a disorderly geometrical arrangement of sheets. As t_{rs} decreases below 1, Fig. 14 shows that the oscillations reduce in amplitude and then vanish entirely. For $t_{rs} \leq 0.5$, fluctuations are virtually nonexistent. Below the oscillatory range of t_{rs}, resheeting has a small effect on the equilibrium solution reached in the calculation. For very small t_{rs} this may reflect accumulated smoothing from the resheeting process, a phenomenon which will be investigated more fully in future work. While the acceptable range of t_{rs} may be increased by enhancing the accuracy of the interpolation scheme

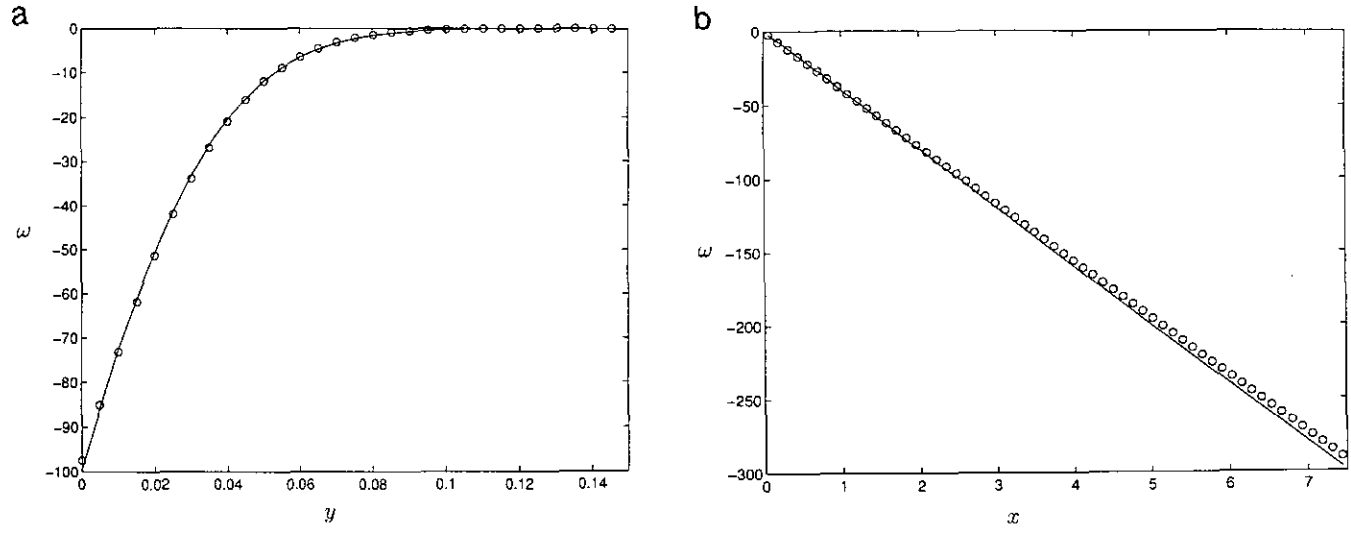

FIG. 13. Comparisons of ω predictions in stagnation flow boundary layer: ———, computed; and O, Falkner–Skan solution. (a) $x = 2.5$; (b) $y = 0$.

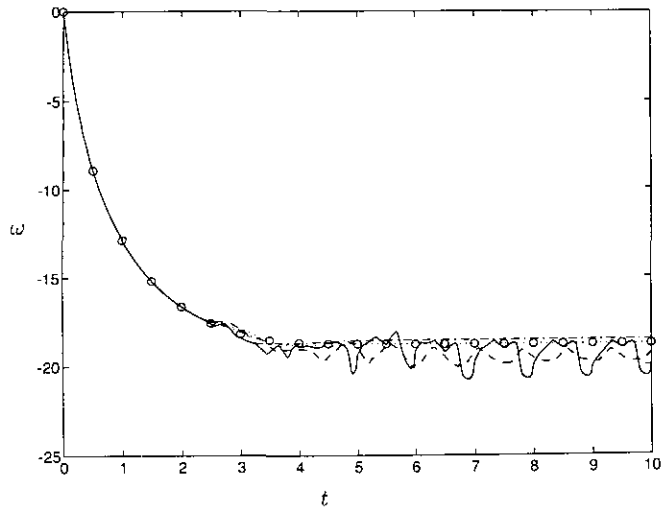

FIG. 14. Effect of t_{rs} on time record of ω at $x = 2.5$, $y = 0.025$ in a Blasius boundary layer: O, $t_{rs} = 0.025$; – · –, $t_{rs} = 0.25$; · · · , $t_{rs} = 0.50$; – – –, $t_{rs} = 0.75$; ———, $t_{rs} = 1$.

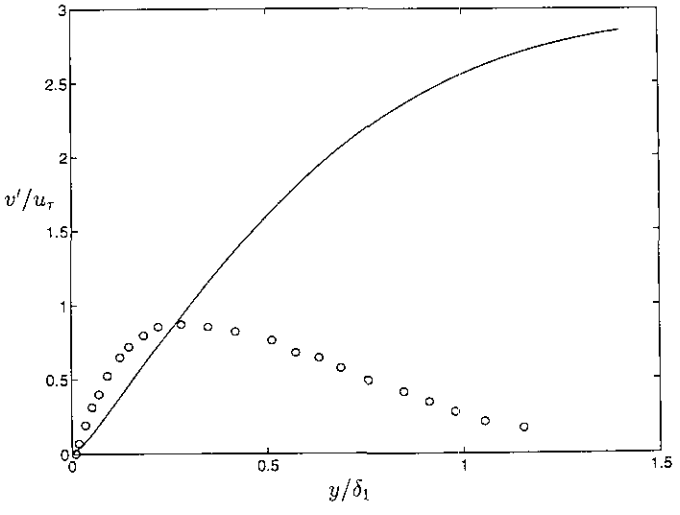

FIG. 16. v'/u_τ: ———, random sheet method; O, turbulent boundary layer in Ref. [25].

(13) and other facets of the method, it is unlikely that the need to resheet can be eliminated. In fact, an analysis of the numerical solutions shows that the amount of overlap of vortex sheets—or, conversely, holes in the vortex element population—increases steadily unless thwarted by regridding. Selection of t_{rs} in applications should be guided by considerations of accuracy and stability, since the computational time needed in regridding using (13) is only a small part of the total. At the same time, to the extent that resheeting is a smoothing process, it is not desirable to continuously resheet, e.g., at every time step. Evidently, t_{rs} should be taken as large as possible but below the onset of oscillations.

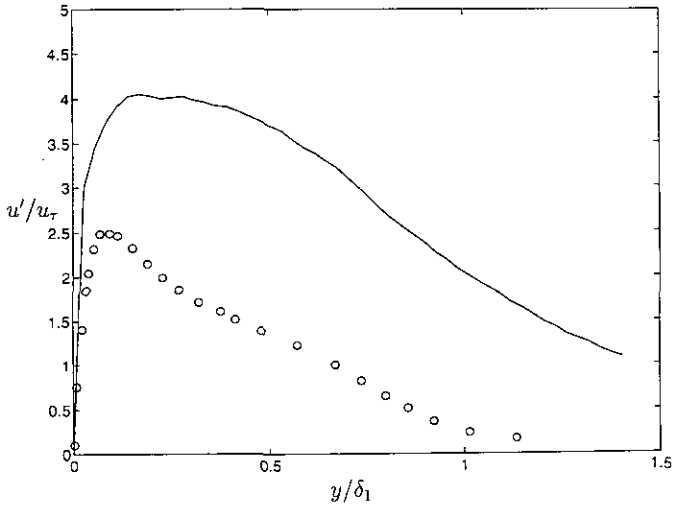

FIG. 15. u'/u_τ: ———, random sheet method; O, turbulent boundary layer in Ref. [25].

The instantaneous realizations of boundary layer flow produced by the present algorithm match the exact similarity solutions without the spatial velocity fluctuations normally associated with the random vortex method. This attribute of the approach may be quantified by the observation that at a fixed point in the boundary layer after steady state conditions are reached, the root-mean-square velocity fluctuation, $u' \equiv (\overline{(u - \bar{u})^2})^{1/2} \ll 1$, where the overbar denotes time averaging. It is instructive to contrast this with u' derived from an equivalent calculation of the Blasius boundary layer using the random sheet method. This is plotted in Fig. 15 with an equivalent plot for v' in Fig. 16. For comparison, the values of u' and v' computed in a turbulent boundary layer simulation by Spalart [25] are also shown. To make the comparisons meaningful, u' and v' are given in wall variables, i.e., scaled by the friction velocity $u_\tau \equiv \sqrt{\nu \partial \bar{u}/\partial y(0)}$, and the abscissa is $y' = y/\delta_1$. These plots show that the pseudo-turbulent energy in the random vortex method dwarfs the naturally occurring energy in a true turbulent flow. In the case of v', the artificial noise is undiminished at the outer edge of the boundary layer due to the peculiarities of (19). An example of the phenomenon displayed in Figs. 15 and 16 may be found in the back step flow calculations reported by Gagnon *et al.* [15], where the turbulent stresses are significantly overpredicted adjacent to boundaries. Evidently, *it is not reasonable to pretend that the chaotic velocity field* associated with the two-dimensional random vortex method is a substitute for real three-dimensional turbulent flow.

6. CONCLUSIONS

The deterministic approach for computing vorticity diffusion developed by Fishelov [13] has been shown to be adaptable to the construction of a vortex sheet method for flows containing solid boundaries. Numerical predictions of channel and bound-

ary layer flows suggest that the approach can be successfully applied to a range of useful applications. The outlook is good that after suitable generalization to take into account spanwise velocities, the method can provide a reliable means of accounting for viscous diffusion in turbulent flow simulations. In particular, it is envisioned that the present technique could be employed in conjunction with a method for simulating the dynamics of three-dimensional vortical structures.

A number of directions to take in improving the approach are worthy of consideration in future work. In particular, the computational efficiency of the algorithm can be enhanced in several ways, including developing fast multipole formulas for Eqs. (23) and (24). Various aspects of the algorithm, including the treatment of the special sets of deforming vortices near the boundaries, the interpolation scheme (14), the resheeting process, the extrapolation condition (10), and the time differencing, may be recast in higher order form to improve accuracy beyond that achieved here.

ACKNOWLEDGMENTS

This research was supported in part by ONR Grant N00014-93-10184 and in part by the Applied Mathematical Sciences Subprogram of the Office of Energy Research, U.S. Department of Energy under Contract DE-AC03-76SF00098 while the author was a visiting professor at the Department of Mathematics, University of California, Berkeley.

REFERENCES

1. C. R. Anderson, A method of local corrections for computing the velocity field due to a distribution of vortex blobs, *J. Comput. Phys.* **61,** 111 (1985).
2. S. B. Baden and E. G. Puckett, A fast vortex method for computing 2D viscous flow, *J. Comput. Phys.* **91,** 278 (1990).
3. T. Beale and A. Majda, High order accurate vortex methods with explicit velocity kernels, *J. Comput. Phys.* **58,** 188 (1985).
4. P. S. Bernard, J. M. Thomas, and R. A. Handler, Vortex dynamics and the production of Reynolds stress, *J. Fluid Mech.* **253,** 385 (1993).
5. A. Cheer, A study of incompressible 2-D vortex flow past a circular cylinder, *SIAM J. Sci. Stat. Comput.* **4,** 685 (1983).
6. A. Cheer, Unsteady separated wake behind an impulsively started cylinder, *J. Fluid Mech.* **201,** 485 (1989).
7. A. J. Chorin, Vortex sheet approximation of boundary layers, *J. Comput. Phys.* **27,** 428 (1978).
8. A. J. Chorin, Hairpin removal in vortex interactions II, *J. Comput. Phys.* **107,** 1 (1993).
9. A. J. Chorin, *Vorticity and Turbulence* (Springer-Verlag, New York, 1994).
10. G. H. Cottet, A particle-grid superposition method for the Navier–Stokes equations, *J. Comput. Phys.* **89,** 301 (1990).
11. G. H. Cottet and S. Mas-Gallic, A particle method to solve the Navier–Stokes system, *Numer. Math.* **57,** 805 (1990).
12. P. Degond and S. Mas-Gallic, The weighted particle method for convection-diffusion equations, Part I: The case of an isotropic viscosity; Part II: The anisotropic case, *Numer. Math.* **53,** 485 (1989).
13. D. Fishelov, A new vortex scheme for viscous flows, *J. Comput. Phys.* **86,** 211 (1990).
14. D. Fishelov, Vortex methods for slightly viscous three-dimensional flow, *SIAM J. Sci. Stat. Comput.* **11,** 399 (1990).
15. Y. Gagnon, A. Giovannini, and P. Hebrard, Numerical simulation and physical analysis of high Reynolds number recirculating flows behind sudden expansions, *Phys. Fluids A* **5,** 2377 (1993).
16. L. Greengard, The numerical solution of the N-body problem, *Comput. Phys.* **Mar/Apr,** 142 (1990).
17. L. Greengard and V. Rokhlin, A fast algorithm for particle simulations, *J. Comput. Phys.* **73,** 325 (1987).
18. W. D. Henshaw, H.-O. Kreiss, and L. G. Reyna, On smallest scale estimates and a comparison of the vortex method to the pseudo-spectral method, *Vortex Dynamics and Vortex Methods,* Lectures in Applied Mathematics, Vol. 28, edited by C. R. Anderson and C. Greengard (Amer. Math. Soc., Providence, RI, 1991), p. 303.
19. P. D. Koumoutsakos, *Direct Numerical Simulations of Unsteady Separated Flows Using Vortex Methods,* Ph.D. thesis, Caltech, 1993.
20. Y. Ogami and T. Akamatsu, Viscous flow simulation using the discrete vortex model—The diffusion velocity method, *Comput. & Fluids* **19,** 433 (1990).
21. E. G. Puckett, Vortex methods: An introduction and survey of selected research topics, in *Incompressible Computational Fluid Dynamics: Trends and Advances,* edited by M. D. Gunzburger and R. A. Nicolaides (Cambridge Univ. Press, Cambridge, UK, 1993), p. 335.
22. G. Russo, A deterministic vortex method for the Navier–Stokes equations, *J. Comput. Phys.* **108,** 84 (1993).
23. H. Schlichting, *Boundary Layer Theory,* 7th ed. (McGraw–Hill, New York, 1979).
24. J. A. Sethian, J.-P. Brunet, A. Greenberg, and J. P. Mesirov, Vortex methods and massively parallel processors. *Vortex Dynamics and Vortex Methods,* Lectures in Applied Mathematics, Vol. 28, edited by C. R. Anderson and C. Greengard (Amer. Math. Soc., Providence, RI, 1991), p. 597.
25. P. R. Spalart, Direct simulation of a turbulent boundary layer up to $R_\theta = 1410$, *J. Fluid Mech.* **187,** 61 (1988).
26. D. M. Summers, A random vortex simulation of Falkner–Skan boundary layer flow, *J. Comput. Phys.* **85,** 86 (1989).
27. F. S. Winckelmans and A. Leonard, Contributions to vortex particle methods for the computation of three-dimensional incompressible unsteady flows, *J. Comput. Phys.* **109,** 247 (1993).